

# RSC Advances



This is an *Accepted Manuscript*, which has been through the Royal Society of Chemistry peer review process and has been accepted for publication.

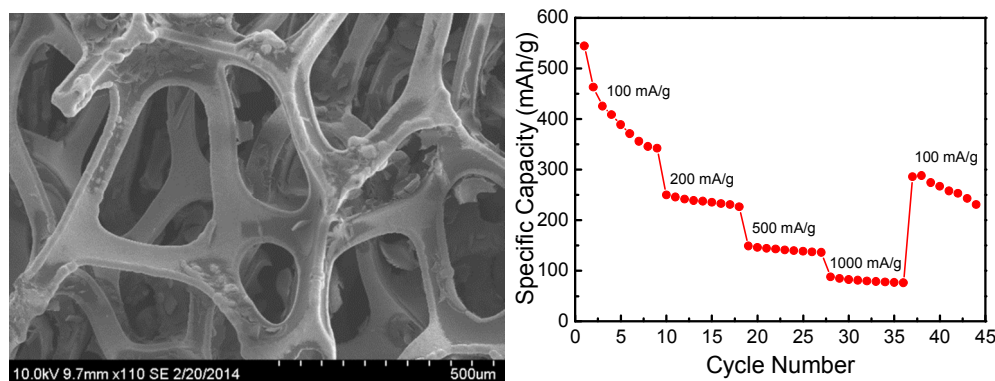
*Accepted Manuscripts* are published online shortly after acceptance, before technical editing, formatting and proof reading. Using this free service, authors can make their results available to the community, in citable form, before we publish the edited article. This *Accepted Manuscript* will be replaced by the edited, formatted and paginated article as soon as this is available.

You can find more information about *Accepted Manuscripts* in the [Information for Authors](#).

Please note that technical editing may introduce minor changes to the text and/or graphics, which may alter content. The journal's standard [Terms & Conditions](#) and the [Ethical guidelines](#) still apply. In no event shall the Royal Society of Chemistry be held responsible for any errors or omissions in this *Accepted Manuscript* or any consequences arising from the use of any information it contains.

## Graphic Abstract

### Direct Growth of Mesoporous Anatase TiO<sub>2</sub> on Nickel Foam by Soft Template Method as Binder-free Anode for Lithium-Ion Batteries



**Graphic Abstract:** Mesoporous TiO<sub>2</sub> directly grown on nickel foam (TiO<sub>2</sub>/Ni) prepared by a one-step soft template method was used directly as a lithium-ion battery anode. The binder-free TiO<sub>2</sub>/Ni shows superior electrochemical properties with a capacity of 341 mAh/g at a current density of 100 mA/g after 10 cycles and 82.4 mAh/g at a current density of 1000 mA/g after 30 cycles.

## ARTICLE

# Direct Growth of Mesoporous Anatase TiO<sub>2</sub> on Nickel Foam by Soft Template Method as Binder-free Anode for Lithium-Ion Batteries

Cite this: DOI: 10.1039/x0xx00000x

Yufeng Jiang,<sup>a</sup> Gen Chen,<sup>a</sup> Xun Xu,<sup>a</sup> Xiaohong Chen,<sup>a,b</sup> Shuguang Deng,<sup>a</sup> Sergei Smirnov,<sup>c</sup> Hongmei Luo,<sup>\*a</sup> and Guifu Zou<sup>\*d</sup>Received 00th January 2012,  
Accepted 00th January 2012

DOI: 10.1039/x0xx00000x

www.rsc.org/

Direct growth of mesoporous TiO<sub>2</sub> on Ni foam via a one-step soft template synthesis was directly used as binder-free anode for lithium-ion batteries. The mesoporous TiO<sub>2</sub> with high specific surface area of 158.8 m<sup>2</sup> g<sup>-1</sup> and average pore size of 5.4 nm formed network-like sheets on the surface of the Ni foam. The binder-free TiO<sub>2</sub>/Ni anode shows improved electrochemical performance with a capacity as high as 341 mAh g<sup>-1</sup> at a current density of 100 mA g<sup>-1</sup> after 10 cycles and 82.4 mAh g<sup>-1</sup> at a current density of 1000 mA g<sup>-1</sup> after 30 cycles. The enhanced electrochemical performance is attributed to the mesoporous structure that shortens the lithium ion diffusion path and facilitates the transport of lithium ion.

## Introduction

Titanium oxide has brought increasing interests due to its potential applications in many fields, such as photocatalysts,<sup>1,2</sup> solar cells,<sup>3,4</sup> and rechargeable lithium batteries.<sup>5,6</sup> Specifically for lithium ion batteries, TiO<sub>2</sub> is highly interested because of its nearly 100% Coulombic efficiency (i.e. its discharge capacity is almost the same as the charge capacity). As compared to the typically used carbonaceous materials, TiO<sub>2</sub> anode operates at ~1.7 V versus Li<sup>+</sup>/Li (~0.1 V for carbon-based anodes), leading to a trade-off in terms of lower overall operating cell voltage but improved capacity retention, lower self-discharge, and enhanced safety and stability.<sup>7</sup> TiO<sub>2</sub> is also chemically stable, inexpensive, nontoxic, and environmentally benign.<sup>8</sup> These properties make TiO<sub>2</sub> particularly attractive for potential large scale energy storage applications. The performance of TiO<sub>2</sub> based material depends strongly on the morphology and porosity of TiO<sub>2</sub>. Different kinds of TiO<sub>2</sub> formulations have been evaluated based on a variety of structural TiO<sub>2</sub> forms including nanotubes, nanowires, nanorods, nanobelts and spheres<sup>9-12</sup> prepared by various methods including seeded growth,<sup>13</sup> hydrothermal,<sup>14</sup> and template-assisted processes.<sup>15</sup> Nano-sized TiO<sub>2</sub> with high surface area, such as mesoporous TiO<sub>2</sub> have been recently found to improve electrochemical properties of TiO<sub>2</sub>.<sup>16</sup>

In order to synthesize mesoporous TiO<sub>2</sub>, templates are commonly used. For most of the hard templates, additional procedures are always required to remove the hard template.<sup>17</sup> Alternative method based on soft templates provides facile synthesis due to the cooperative self-assembly. In such processes, inorganic titanium precursor blends with organic surfactant (the structure directing agent) and further cooperatively assembles with surfactant due to a combination of covalent and hydrogen bonding, as well as, Coulombic forces. Most organic surfactants will decompose during the heat

treatment and thus are removed during calcination. The facile one-step process makes the soft template method more attractive for building mesoporous structures.

TiO<sub>2</sub>, as majority of other metal oxides, suffers from low electronic conductivity, which negatively affects its electrochemical performance. One common way to circumvent that is to add a conductive agent and binder. However, introduction of non-active material diminishes the fraction of active material on the electrode and that would lead to the loss of a fraction of total capacity based on pure active material. As one of the alternative ways to solve this problem, binder-free electrode has been introduced.<sup>18-20</sup> For a binder-free electrode, the active material is directly grown on the current collector, resulting in tighter contact between the current collector and the active material and eliminates the need for additional binder.

In this paper, we report the direct growth of mesoporous anatase TiO<sub>2</sub> nanocrystals on Ni foam by a soft template method. Unlike the conventional way, preparation of the active material and fabrication of the electrode are accomplished in one-step. The binder-free TiO<sub>2</sub>/Ni anode with small fraction of residual carbon shows improved conductivity with no sacrifice in total capacity. The binder-free TiO<sub>2</sub>/Ni anode demonstrates the capacity as high as 341 mAh g<sup>-1</sup> at a current density of 100 mA g<sup>-1</sup> and 82.4 mAh g<sup>-1</sup> at the current density of 1000 mA g<sup>-1</sup>.

## Experimental

### Synthesis method

All the reagents were purchased and directly used without further purification. Titanium tetraisopropoxide (TTIP) was used as the Ti source and organic surfactant Pluronic F127 (M<sub>w</sub> = 12600) was used as the soft template. Typically, 2.84 g of TTIP and 2.54 g of Pluronic F127 was added to 10.3 mL of ethanol and 2 mL of HCl (37%). A clear sol was obtained by continuous stirring at room temperature for 2 h. Ni foam (MTI

Corp.) was cut into small pieces ( $\sim 1 \text{ cm}^2$ ) then washed by acetone and dried at  $80 \text{ }^\circ\text{C}$ . To prepare  $\text{TiO}_2/\text{Ni}$ , small pieces of Ni foam were immersed in the sol for 1 min and then transferred into crucible boat and heated at  $450 \text{ }^\circ\text{C}$  or  $650 \text{ }^\circ\text{C}$  in box furnace for 3 h (heating rate  $2 \text{ }^\circ\text{C}/\text{min}$ ) in air. Finally, the Ni foam covered with  $\text{TiO}_2$  was sonicated in deionized water to remove the unbound materials and followed by drying in vacuum oven at  $80 \text{ }^\circ\text{C}$  overnight. The  $\text{TiO}_2$  powder was prepared by same procedure but without Ni foam.

### Characterization

The phase and crystal structure of the samples were studied by X-ray diffraction (XRD) using a Rigaku Miniflex II X-ray powder diffractometer with CuK $\alpha$  radiation. The morphology and microstructure were characterized by scanning electron microscopy (SEM, S-3400NII) and transmission electron microscopy (TEM, H-7650). The elemental content was evaluated by energy dispersive X-ray spectroscopy (EDS) on SEM. Nitrogen adsorption-desorption isotherms were collected by using ASAP 2020 chemisorption analyzer. Barrett-Joyner-Halenda (BJH) methods were used to estimate the pore size and pore-size distribution.

### Electrochemical Measurement

Electrochemical properties were measured using CR-2032 coin cells. A piece of metallic lithium foil ( $\sim 1 \text{ cm}^2$ ) was used as the counter electrode.  $\text{TiO}_2/\text{Ni}$  was directly used as the working electrode. The weight of active material was measured by the difference of the Ni foam measured before and after the synthesis process. The weight gain caused by oxidation of Ni was measured and deducted. For each of the electrodes, the mass loading of active material is about 1 mg. The solution of 1 M  $\text{LiPF}_6$  in a mixture of ethylene carbonate (EC) – dimethyl carbonate (DMC) (1:1 by volume) was used as the electrolyte. Coin cells were assembled in an argon-filled dry glove box (Vigor Gas Purification Technologies, Inc.). Galvanostatic charge/discharge cycling performance was evaluated on an LAND Battery Tester CT2001A with the potential range of 1.0–3.0 V (vs.  $\text{Li}^+/\text{Li}$ ) at different current densities. Cyclic voltammetry (CV) was carried out using a Princeton Applied Research Versa STAT4 electrochemical workstation. The electrochemical impedance measurement was performed on fresh coin cell samples at zero bias and with 5 mV AC amplitude on a CHI-680A workstation (CH Instruments, Inc).

## Results and discussion

### Structural Analysis

The XRD patterns of  $\text{TiO}_2$  heated at  $450 \text{ }^\circ\text{C}$  and  $650 \text{ }^\circ\text{C}$  are shown in Fig. 1. The sharp narrow peaks of the sample heated at  $650 \text{ }^\circ\text{C}$  indicate that the sample has a larger particle size other than the broader peaks for the sample heated at  $450 \text{ }^\circ\text{C}$ . Both patterns showed the corresponding peaks of anatase phase of  $\text{TiO}_2$  (JCPDS No. 65-5714). Two peaks of  $\text{NiTiO}_3$  were observed at  $\sim 35$  degree (marked as stars in Fig.1) for the sample heated at  $650 \text{ }^\circ\text{C}$ , which may be due to side reactions between  $\text{TiO}_2$  and Ni foam at high temperature. To eliminate impurities and get pure  $\text{TiO}_2$ , a calcination temperature was tuned to  $450 \text{ }^\circ\text{C}$ . The XRD pattern of  $\text{TiO}_2$  heated at  $450 \text{ }^\circ\text{C}$  showed no impurity and good crystallinity with smaller particle size.

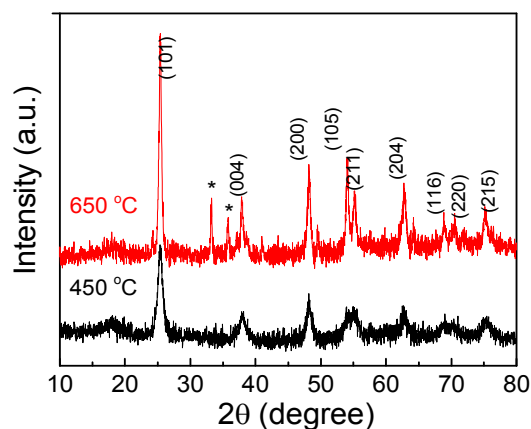


Fig.1 XRD patterns of  $\text{TiO}_2$  heated at  $450 \text{ }^\circ\text{C}$  and  $650 \text{ }^\circ\text{C}$  for 3 h.

As shown in Fig. 2(a), nitrogen adsorption-desorption isotherm of the mesoporous powder presents a type IV hysteresis loop with a Brunauer-Emmet-Teller (BET) surface area of  $158.8$  and  $82.9 \text{ m}^2 \text{ g}^{-1}$  for  $\text{TiO}_2$  heated at  $450 \text{ }^\circ\text{C}$  and  $650 \text{ }^\circ\text{C}$ , respectively. Based on the BJH adsorption, the pore size distribution was calculated and the curves are shown in Fig. 2(b). The average pore sizes of the mesoporous  $\text{TiO}_2$  samples heated at  $450 \text{ }^\circ\text{C}$  and  $650 \text{ }^\circ\text{C}$  are 6 nm and 13 nm, respectively. The decrease of the average pore size may be attributed to residual carbon in the mesoporous  $\text{TiO}_2$  at low calcination temperature, which is further confirmed by the TEM images. The sample heated at  $450 \text{ }^\circ\text{C}$  has a more typical type IV plot which confirms the mesoporous nature of  $\text{TiO}_2$ . The higher surface area and smaller pore sizes of  $\text{TiO}_2$  heated at  $450 \text{ }^\circ\text{C}$  are believed to benefit the fast diffusion of lithium ions.

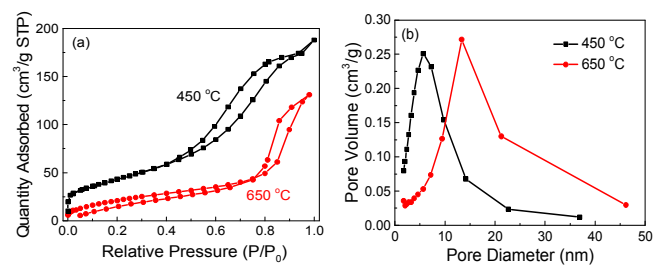
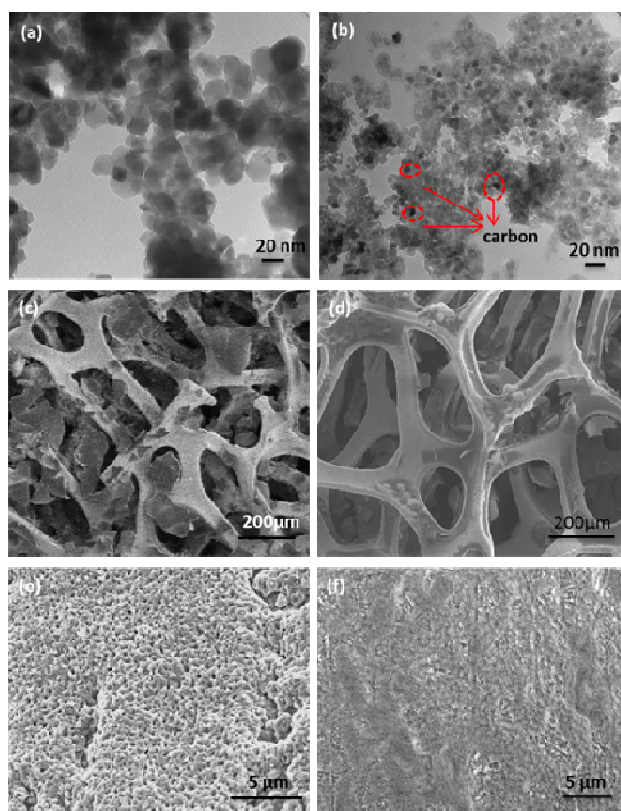


Fig. 2 (a) Nitrogen adsorption and desorption isotherm plots of porous  $\text{TiO}_2$  heated at  $450 \text{ }^\circ\text{C}$  and  $650 \text{ }^\circ\text{C}$ ; (b) BJH adsorption pore size distribution curves of  $\text{TiO}_2$  heated at  $450 \text{ }^\circ\text{C}$  and  $650 \text{ }^\circ\text{C}$ .

TEM images of mesoporous  $\text{TiO}_2$  powder prepared at  $650$  and  $450 \text{ }^\circ\text{C}$  are shown in Fig. 3(a,b) and indicate that  $\text{TiO}_2$  heated at  $650 \text{ }^\circ\text{C}$  has much bigger domain size ( $\sim 30 \text{ nm}$ ) while the domain size of the  $\text{TiO}_2$  heated at  $450 \text{ }^\circ\text{C}$  is only  $\sim 10 \text{ nm}$ , which is consistent with XRD patterns. The increase of domain size is mainly attributed to the increase of heating temperature, which enhanced agglomeration of particles. The smaller domain size is believed to be more favorable for lithium insertion.<sup>21</sup> The carbon content was determined as 10.5 wt% by EDS (supporting information, Fig. S1). Fig.3(c,d) shows typical morphologies of mesoporous  $\text{TiO}_2/\text{Ni}$  over a large area, indicating that the surface of Ni foam is well covered by a sheet of porous  $\text{TiO}_2$ . The magnified images in Fig. 3(e,f) suggest a porous network-like sheets morphology of the  $\text{TiO}_2$  and a good connection between  $\text{TiO}_2$  and the Ni foam.



**Fig. 3** TEM images of TiO<sub>2</sub> powder heated at (a) 650 °C and (b) 450 °C; SEM images for TiO<sub>2</sub>/Ni heated at 650 °C (c,e) and 450 °C (d,f), respectively.

### Electrochemical Performance

The electrochemical properties of TiO<sub>2</sub>/Ni were investigated by galvanostatic charging and discharging in a voltage range of 1.0–3.0 V (vs. Li<sup>+</sup>/Li), which is consistent with typical discharge/charge voltage profiles of TiO<sub>2</sub>. The Li insertion/extraction reaction in TiO<sub>2</sub> can be written as: TiO<sub>2</sub> + xLi<sup>+</sup> + xe<sup>-</sup> ↔ Li<sub>x</sub>TiO<sub>2</sub>, where x is the amount of inserted Li<sup>+</sup> in anatase TiO<sub>2</sub>.<sup>22</sup> As shown in Fig. 4, 544 mAh g<sup>-1</sup> and 255 mAh g<sup>-1</sup> of capacity were achieved for the samples heated at 450 °C and 650 °C, respectively, in the first cycle. Capacity loss was detected for both samples on the second cycle, which is mainly attributed to the interfacial reaction between TiO<sub>2</sub> and the electrolyte and the phase change, which are common to most lithium intercalation hosts.<sup>23,24</sup> High capacity of 520 mAh g<sup>-1</sup> for TiO<sub>2</sub> for the first cycle with large irreversible capacity loss was also observed, which might be also caused by the reduction of surface OH groups and residual surface H<sub>2</sub>O by Li atoms.<sup>25,26</sup> Both TiO<sub>2</sub>/Ni samples have large capacity loss on the second cycle (21.1% for TiO<sub>2</sub>/Ni heated at 450 °C and 11.3% for TiO<sub>2</sub>/Ni heated at 650 °C) but the rate of loss declines with consecutive cycles. About 341 mAh g<sup>-1</sup> and 182 mAh g<sup>-1</sup> of the capacity remains for 450 °C and 650 °C, respectively, after 10 cycles. For the sample heated at 650 °C, a potential plateau at around 1.75 V with a sloped region of 1.75–1.0 V were observed during the first discharge process, and a voltage plateau at around 1.92 V was observed in the first charge process, which is slightly higher than the normal charge plateaus at 1.88 V. The voltage plateaus at 1.75 and 1.92 V correspond to lithium-ion intercalation into and deintercalation from the interstitial octahedral sites of anatase TiO<sub>2</sub>,

respectively.<sup>27</sup> The discharge capacity originates from the reduction of Ti(IV) to Ti(III) with intercalation of the lithium ions, whereas the charge capacity originates from the oxidation of Ti.<sup>28</sup> For mesoporous TiO<sub>2</sub>/Ni heated at 450 °C, the large region of slope indicates a huge contribution to capacity from the surface storage of lithium due to the large BET surface area.<sup>20</sup> No obvious plateaus could be observed, which may also be due to the lower crystallinity of TiO<sub>2</sub> annealed at 450 °C. The results are comparable to TiO<sub>2</sub> with porous structure reported previously.<sup>29–30</sup>

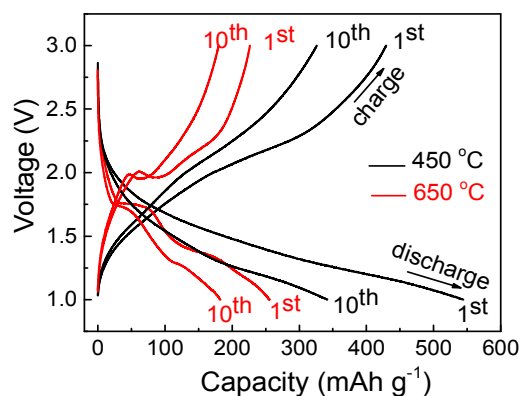


**Fig. 4** The initial and 10<sup>th</sup> cycle discharge/charge voltage profiles at a constant current density of 0.1 A g<sup>-1</sup> for TiO<sub>2</sub>/Ni heated at 450 °C and 650 °C, respectively.

The Nyquist plots of both samples are shown in Fig. 5, from where it can be observed that the charge-transfer resistance (the diameter of the semicircle in the medium-frequency region) decreased from 145 Ω for TiO<sub>2</sub>/Ni heated at 650 °C to 39 Ω for TiO<sub>2</sub>/Ni heated at 450 °C. We associate this drastic suppression of the resistance with the residual carbon, more of which survives at lower heating temperature.

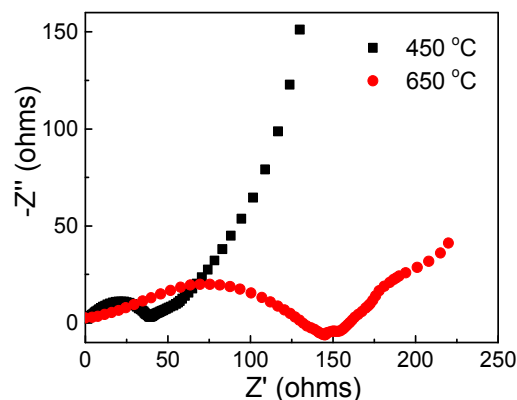


**Fig. 5** Nyquist plots for TiO<sub>2</sub>/Ni anodes heated at 450 °C and 650 °C, respectively.

The rate performance of TiO<sub>2</sub>/Ni heated 450 °C at 100 mA g<sup>-1</sup> and higher current densities are shown in Fig. 6. The capacities are 249, 149, and 88 mAh g<sup>-1</sup> at current densities of 200, 500, 1000 mA g<sup>-1</sup>, respectively. When the current density returned to 100 mA g<sup>-1</sup>, the specific capacity rebounded to 285 mAh g<sup>-1</sup>, which corresponds to 83.5% retention rate. The small reductions of capacity during the cycling tests at different current densities indicate good cycling performance. The Coulombic efficiency of 80% at the first cycle but drastically

increased to practically 100% after five cycles, indicating a good reversibility. The initial low efficiency is probably due to the slow activation process.

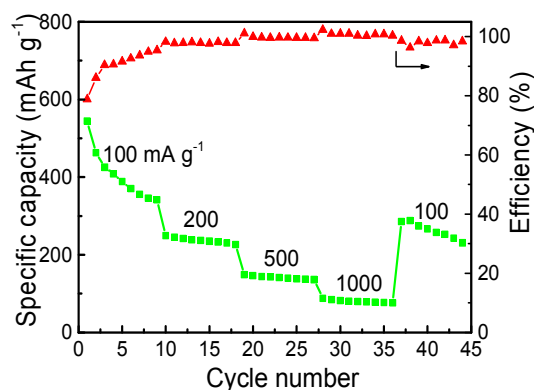


**Fig. 6** Rate performance of mesoporous TiO<sub>2</sub>/Ni heated at 450 °C and the corresponding Coulombic efficiency.

## Conclusions

In summary, mesoporous TiO<sub>2</sub>/Ni has been prepared by direct growth of mesoporous TiO<sub>2</sub> nanocrystal on Ni foam via a facile one-step soft template synthesis method and demonstrated excellent electrochemical properties when used as binder-free anode for lithium ion batteries. The mesoporous TiO<sub>2</sub>/Ni calcined at 450 °C showed better performance than that at elevated temperature due to the mesoporous character of TiO<sub>2</sub> tightly bound to Ni and reduced resistance due to residual carbon from the template removal. The capacity of mesoporous TiO<sub>2</sub>/Ni is as high as 341 mAh g<sup>-1</sup> after 10 cycles at a current density of 100 mA g<sup>-1</sup> and 82.4 mAh g<sup>-1</sup> at a current density of 1000 mA g<sup>-1</sup> after 30 cycles. The enhanced electrochemical performance is attributed to the mesoporous structure shortening the lithium ion diffusion path and facilitating the transport of lithium, and the good conductivity provided by residual carbon.

## Acknowledgements

H. Luo acknowledges the funding support from NSF/CMMI NanoManufacturing Program under Grant No. 1131290 and the office of Vice President for Research at NMSU. X. X. acknowledges the GREG award. X. Chen acknowledges the support from the China Scholarship Council. G. Zou acknowledges the support from the National Natural Science Foundation of China (21101110), Jiangsu Fund for Distinguished Young Scientist (BK20140010), Jiangsu Specially-Appointed Professor Program (SR1080042), and Jiangsu Scientific and Technological Innovation Team (2013).

## Notes and references

<sup>a</sup>Department of Chemical and Materials Engineering, New Mexico State University, Las Cruces, New Mexico 88003, USA. E-mail: hluo@nmsu.edu; Fax: +1-575-646-7706; Tel: +1-575-646-4204

<sup>b</sup>State Key Laboratory of Chemical Resource Engineering, Key Laboratory of Carbon Fiber and Functional Polymers, Ministry of Education, Beijing University of Chemical Technology, Beijing, P. R. China

<sup>c</sup>Department of Chemistry and Biochemistry, New Mexico State University, Las Cruces, New Mexico 88003, USA.

<sup>d</sup>College of Physics, Optoelectronics and Energy & Collaborative Innovation Center of Suzhou Nano Science and Technology, Soochow University, Suzhou 215000, P. R. China. E-mail: [zouguifu@suda.edu.cn](mailto:zouguifu@suda.edu.cn); Fax: +86-512-65228130; Tel: +86-512-65228130

†Electronic Supplementary Information (ESI) available: EDS of mesoporous TiO<sub>2</sub> heated at 450 °C. See DOI: 10.1039/b000000x/

1. M. Mrowetz, W. Balcerski, A. J. Colussi, and M. R. Hoffmann, *J. Phys. Chem. B*, 2004, **108**, 17269.
2. J. C. Yu, J. Yu, W. Ho and L. Zhang, *Chem. Commun.*, 2001, **19**, 1942.
3. K. Hara, Kazuhiro Sayama, Y. Ohga, A. Shinpo, S. Suga and H. Arakawa, *Chem. Commun.*, 2001, **6**, 569.
4. Y. C. Tu, J. F. Lin, W. C. Lin, C. P. Liu, J. J. Shyue and W. F. Su, *CrystEngComm*, 2012, **14**, 4772.
5. J. Kim and J. Cho, *J. Chem. Soc.*, 2007, **154**, A542.
6. V. Subramanian, A. Karki, K. I. Gnanasekar, F. P. Eddy, B. Rambabu, *J. Power Sources*, 2006, **159**, 186.
7. L. Fu, H. Liu, H. Zhang, C. Li, T. Zhang, Y. Wu and H. Wu, *J. Power Sources*, 2006, **159**, 219.
8. Juan Su, Xiaoxin Zou, Guo-Dong Li, Yan-Mei Jiang, Yang Cao, Jun Zhao, Jie-Sheng Chen, *J. Phys. Chem. C*, 2009, **113**, 21258.
9. T. Kasuga, M. Hiramatsu, A. Hoson, T. Sekino, and K. Niihara, *Langmuir*, 1998, **14**, 3160.
10. N. Q. Wu, J. Wang, D. N. Tafen, H. Wang, J. G. Zheng, J. P. Lewis, X. G. Liu, S. S. Leonard and A. Manivannan, *J. Am. Chem. Soc.*, 2010, **132**, 6679.
11. J. H. Park, S. Kim and A. J. Bard, *Nano Lett.*, 2006, **6**, 24.
12. T. H. Eun, S. H. Kim, W. J. Jeong, S. J. Jeon, S. H. Kim and S. M. Yang, *Chem. Mater.*, 2009, **21**, 201.
13. M. X. Xia, Q. L. Zhang, H. X. Li, G. Z. Dai, H. C. Yu, T. H. Wang, B. S. Zou and Y. G. Wang, *Nanotechnology*, 2009, **20**, 055605.
14. X. Y. Hu, T. C. Zhang, Z. Jin, S. Z. Huang, M. Fang, Y. C. Wu and L. D. Zhang, *Cryst. Growth Des.*, 2009, **9**, 2324.
15. C. Bae, Y. J. Yoon, H. Yoo, D. Han, J. H. Cho, B. H. Lee, M. M. Sung, M. G. Lee, J. Y. Kim and H. Shin, *Chem. Mater.*, 2009, **21**, 2574.
16. H. S. Zhou, D. L. Li, M. Hibino and I. Honma, *Angew. Chem. Int. Ed.*, 2005, **44**, 797.
17. S. I. Matsushita, T. Miwa, D. A. Tryk, and A. Fujishima, *Langmuir*, 1998, **14**, 6441.
18. Y. Li, M. A. Trujillo, E. Fu, B. Patterson, L. Fei, Y. Xu, S. Deng, S. Smirnovc and H. Luo, *J. Mater. Chem. A*, 2013, **1**, 12123.
19. Z. Chen, D. Weng, X. Wang, Y. Cheng, G. Wang and Y. Lu, *Chem. Commun.*, 2012, **48**, 3736.
20. Z. Chen, D. Zhang, X. Wang, X. Jia, F. Wei, H. Li and Y. Lu, *Adv. Mater.*, 2012, **24**, 2030.
21. M. Wagemaker, W. J. H. Borghols and F. M. Mulder, *J. Am. Chem. Soc.*, 2007, **129**, 4323.
22. K. Saravanan, K. Ananthanarayanan, P. Balaya, *Energy Environ. Sci.*, 2010, **3**, 939.
23. G. Sudant, E. Baudrin, D. Larcher and J.-M. Tarascon, *J. Mater. Chem.*, 2005, **15**, 1263.
24. Y. G. Guo, Y. S. Hu, J. Maier, *Chem. Commun.*, 2006, **26**, 2783.

25. Chen, J. S.; Tan, Y. L.; Li, C. M.; Cheah, Y. L.; Luan, D.; Madhavi, S.; Boey, F. Y. C.; Archer, L. A.; Lou, X. W. *J. Am. Chem. Soc.*, 2010, **132**, 6124.
26. Das, S. K.; Bhattacharyya, A. J. *J. Phys. Chem. C*, 2009, **113**, 17367.
27. D. Dambournet, I. Belharouak, K. Amine, *Chem. Mater.*, 2010, **22**, 1173.
28. S. Sodergren, H. Siegbahn, H. Rensmo, H. Lindstrom, A. Hagfeldt, S. E. Lindquist, *J. Phys. Chem. B*, 1997, **101**, 3087.
29. J. Ming, Y. Q. Wu, S. Nagarajan, D. J. Lee, Y. K. Sun, F. Y. Zhao, *J. Mater. Chem.*, 2012, **22**, 22135.
30. J. F. Ye, W. Liu, J. G. Cai, S. A. Chen, X. W. Zhao, H. H. Zhou, L. M. Qi, *J. Am. Chem. Soc.*, 2011, **133**, 933.